Direct Plasmadynamic Conversion of Plasma Thermal Power to Electricity

R. M. Mayo and R. L. Mills
BLP Inc.
Cranbury, NJ 08512

The generation of electrical energy using direct plasmadynamic conversion (PDC) is studied experimentally for small-scale, chemically-assisted plasmas (CA-plasma) for the first time. Glow discharge and microwave generated plasma sources are operated at power levels on the order of a few to 50 Watts in the discharge case and up to 12.83 W/cm^3 in the microwave case. Extracted power approaching ¼ W has been achieved as a demonstration. It is envisioned that such a system may be readily scaled to a few hundred Watts to several 10's of kW output power for microdistributed commercial applications (e.g. household, automotive, light industry, and space based power). Three quarter in. long by 0.040 in. diameter cylindrical PDC electrodes have been tested in a 10 – 50 W direct current, glow discharge plasma device with He or Ar as the working gas at 0.3 – 3.0 Torr. The PDC anode was magnetized in the range of 0 – 700 G with a 1.5 inch water cooled Helmholtz electromagnet. Open circuit voltages up to 6.5 V were obtained across the PDC electrodes at 1 Torr He and 350 G field. The collector voltage was shown to be a function of applied magnetic field strength, B, and peaking at about 300 G. A variety of resistive loads were connected across the PDC electrodes, extracting continuous electrical power up to 0.44 mW. The power/load curve peaks at 0.44 mW for a 20 kΩ load indicating the impedance matching condition with the plasma source. The most severe limitation to collector output performance is shown to be plasma conductivity. Collector power drops sharply with increasing neutral gas fill pressure in the glow discharge chamber at constant discharge current indicating that electron collisions with neutral gas atoms are responsible for the reduction in conductivity. Scale-up to higher power has been achieved with the use of a microwave plasma generator. A ¾ in. long by 0.094 in. dia. PDC anode was magnetized to ~140 G resulting in open circuit PDC voltages in excess of 11.5 V for He plasmas at ~0.75 – 1 Torr and 50 sccm flow. Due to higher conductivity, load matching was now obtained at ~600 Ω. Langmuir probe results indicate good agreement between the conductivity change and the electron to neutral density ratio scale-up. For this source and electrode configuration, PDC power as high as ~200 mW was demonstrated in He at 0.75 Torr for a microwave input power density of ~8.55 W/cm^3. Considering an electron mean free path as the scale for collector probe influence in the plasma, the peak extracted power density is ~1.61 W/cm^3, corresponding to a volumetric conversion efficiency of ~18.8%.

Introduction

High temperature plasmas possess a substantial inventory of energy stored in the thermal and/or kinetic components of plasma ions, electrons, and in some cases neutral gas particles in some weakly ionized plasmas. There is obvious incentive in devising methods and technologies to efficiently extract this energy and convert it to a more useful form. Most often, conversion to electrical energy is desired as this form is readily stored and transmitted, and is efficiently converted to mechanical work at the delivery site.

A number of plasma energy conversion schemes have been studied in the four plus decades of controlled thermonuclear fusion research. At high temperature (as that produced in the blanket material of high power D-T fusion reactor) a thermal steam cycle [1,2] is usually considered the most practical energy extraction means as the bulk (80%) of the energy release is in the form of chargless neutrons. Thermal steam cycles are robust, reliable, proven technologies, and are well established as the work horse of modern electrical power delivery. Yet, the conversion efficiency is limited and high coolant temperatures are required. Furthermore, costs are prohibitive for the use of steam cycles in small, distributed power sources.

Direct conversion of plasma charged particle kinetic to electric energy [3] may represent an attractive alternative to the steam cycle for at least several plasma systems of great interest including; (a) the D-T fusion reactor (as a "topping" unit to extract the 20% of fusion energy in high energy charged particles), (b) advanced, a-neutronic fueled fusion reactors, and (c) chemically assisted (CA)-plasma cells [4 – 6]. In fusion reactors, the fully ionized, high temperature (up to 10 – 15 keV) plasma energy may be readily extracted by direct, electrostatic means, thereby converting charged particle kinetic energy to electrostatic potential energy via decelerating electrodes [3]. Whereas for CA-plasma cell devices, possessing only weakly ionized and relatively cold plasmas, conversion methods more compatible with a fluid environment like MHD converters [7] may be required to extract stored energy.

Herein, we demonstrate the plasmadynamic conversion (PDC) of plasma thermal to electrical energy from discharge and microwave plasmas as a illustration of power extraction from CA-plasma cells. As in MHD conversion, PDC extracts stored plasma energy directly. Unlike MHD, however, PDC does not require plasma flow. Instead, power extraction by PDC exploits the potential difference established between a magnetized and an unmagnetized electrode [8] immersed in a plasma to drive current in an external load and, thereby, extract electrical power directly from the stored plasma thermal energy. For the first time, a substantial quantity of electrical power is extracted (up to 0.4 mW in the discharge plasma case and up to 220 mW in the microwave case). This scale-up is concomitant with a like increase in the plasma to neutral density ratio. Further power scale-up to commercially appropriate power levels is now realizable. The engineering relationships learned from these simulation studies can be applied to converting the thermal power from CA-plasmas to electrical power.

Theory

When an isolated (floating) conductor is inserted into a thermal plasma, it is predicted to attain the potential

$$V_f = V_p - \left[\frac{1}{2}\ln\left(\frac{2M}{\pi m}\right)\right]\frac{kT_e}{e} \qquad - 1$$

referred to as the floating potential, by the steady, one-dimensional electron equation of motion (EOM) and fixed ions unimpeded by the sheath potential. Here, V_p is the plasma potential, kT_e is the electron temperature, and M and m are the ion and electron masses, respectively. In the presence of a magnetic field of intermediate strength (*i.e.* sufficient to magnetize electrons but not ions) and parallel to the surface of the conductor, electron collection at the conductor is substantially reduced and the local floating potential is altered. While a complete and general description is rather involved, sufficient insight into the influence of magnetization can be gained by examining the collection of electron current near the space (plasma) potential [9]. This approach is justified since the impediment of electron current to a floating probe results in a modified floating potential, V_{fm}, such that $V_f < V_{fm} < V_p$ and approaching V_p. As magnetization (B) is provided only completely parallel to the probe surface facing the plasma, we consider only diffusive transport of electrons to the probe. In contrast to the situation described by Eq. 1, collisions are now required to allow an electron current to the probe. Current continuity [9] dictates that the electron density within one mean collision distance to the probe, n′, is given by

$$n' = \frac{n_o}{1+\beta}$$

with

$$\beta = \frac{A_p \bar{v}}{16\pi CD}\left(1+\Omega^2\right)^{1/2}$$

where n_o is the plasma electron density far from the probe in the bulk plasma, A_p is the probe surface area, $\bar{v}$ is the average electron speed, C is the probe capacitance with respect to the surface at infinity with charge density n_o (taken to be at the plasma-sheath boundary), D is the mass diffusivity in the absence of B, Ω is the electron magnetization parameter ($\Omega = eB/m\nu_{en}$), and ν_{en} is the electron-neutral particle collision frequency. Only electron-neutral collisions need to be considered as neutral particles by far dominate the scattering interactions with electrons as the pressures considered here.

Since the probe is aligned parallel to B, the effective collision distance becomes the electron gyro-radius, r_L. Since x_s (sheath thickness) $<< r_L << \lambda$ (mean free path), collisions may be ignored in the last gyro-step to the probe so that the Boltzmann relation applies

$$n = n'\exp\left[\frac{e}{kT_e}(V - V_p)\right] \qquad - 2$$

Balancing electron and ion currents, then, for the magnetized floating probe yields

$$V_{fm} = V_p - \frac{kT_e}{2e}\ln\left(\frac{2M}{\pi m}\right) + \frac{kT_e}{e}\ln(1+\beta) \qquad - 3$$

This expression now replaces Eq.1 in the magnetized as well as unmagnetized case (B=0) since $\beta_o = \beta(\Omega = 0) \neq 0$ to include the effect of collisions on electron current in the limit $B \rightarrow 0$.

Plasmadynamic conversion (PDC) of thermal plasma energy to electricity is achieved by inserting two floating conductors in a plasma, one magnetized, the other unmagnetized. The potential difference between the two conductors (now appropriately referred to as electrodes) is given by the difference in unmagnetized and magnetized floating potential as described by Eq. 3 with β_o and β, respectfully. Referring to this potential difference as the open circuit PDC voltage, V_o, we have

$$V_o = \frac{kT_e}{e}\ln\left(\frac{1+\beta}{1+\beta_o}\right)$$

Since β & β_o >>1, the probe area and capacitance no longer enter the PDC voltage expression, so that

$$V_o = \frac{kT_e}{2e}\ln(1+\Omega^2) \qquad - 4$$

In a strongly magnetized plasma (Ω~20) at 2 eV, a respectable V_o~6 V can be expected. The ln B dependence at large B is expected from the Boltzmann relation (Eq.2) as the electron density reaching the probe decreases as 1/B for large field strength. I should be noted here that in general the conditions at the magnetized and unmagnetized probe may be different so that even when β & β_o >>1, the logarithmic term in Eq. 4 may retain the dependencies

$$\frac{\beta}{\beta_o} = \frac{A_p}{A_{p_o}}\frac{\bar{v}}{\bar{v}_o}\frac{C_o}{C}\frac{D_o}{D}(1+\Omega^2)^{1/2}$$

Where the subscript "o" refers to conditions at the unmagnetized electrode. Increasing the magnetized electrode area or electron thermal speed at the electrode should incur increased PDC voltage, while the same should be expected with a reduction in effective probe capacitance or mass diffusivity near the probe. Modification to the probe surface area though is often the parameter in the most readily controlled by the experimenter. In addition, electrostatic potential difference generated by thermal gradients in the plasma have been neglected here. Placing the electrodes in regions of the plasma at different temperatures can further increase the collection potential [10].

Shorting the PDC electrodes with the load, R_L, allows the circuit to be completed, and current and power flow to the external load. The PDC source is necessarily loaded by this action, thereby reducing the source voltage to V_o-iR, where R is the internal resistance of the source (*i.e.* plasma & PDC electrode system). Assigning the loaded PDC voltage as

$$V_{PDC} = V_o - iR$$

where $i = V_o/(R + R_L)$, the extracted power is found

$$P_{PDC} = \frac{R_L}{(R + R_L)^2} V_o^2$$

As expected, the impedance matching condition $R = R_L$ determines the peak extracted power

$$P_{max} = \frac{1}{4R_L} V_o^2 \qquad - 5$$

In the V_o~6 V example from above and with R_L~10 kΩ, a maximum extracted power of 0.9 mW can be realized. Attaining 1 W of extracted power from PDC under these plasma conditions requires a source impedance matched to the load at R_L~9 Ω.

Experimental Apparatus

Two separate PDC experiments are described here. In the first, a DC glow type discharge plasma was generated in a 1 in. diameter (OD) by 12 in. glass tube. In the second, a 1.5 kW maximum output power microwave generator was used to generate plasma in a quartz applicator tube of similar dimensions. In both experiments, one magnetized (anode) PDC electrode and one unmagnetized (cathode) electrode was inserted into the main part of the discharge. Open circuit and resistive load tests were performed to obtain V_o as well as loaded PDC voltages (V_{PDC}), current, and power as a function of operating and plasma parameters.

A schematic of the glow discharge tube apparatus is shown in Fig. 1. A gas discharge was initiated in He or Ar at 0.3 – 3.0 Torr between a set of ¾ in. disk discharge electrodes. The discharge anode was welded to a 3/8 in. stainless steel (SS) tube to allow

concentric access for the PDC anode. The discharge cathode was likewise welded to a 3/8 in. SS tube that served both as a vacuum pumping port and electrode. This side of the discharge power delivery was grounded to the experiment platform and power supply ground. The discharge electrodes were separated by 20 cm and are powered by a 600 V, 2 A DC power supply (Xantrex XFR600-2) which produced DC glow plasmas with discharge currents in the range 0.02 – 150 mA at 300 – 540 V. Typical discharge operating power for the experiments described here was 10 – 50 W. A 1 kΩ, 225 W resistor was placed in series with the power supply to limit the discharge current and stabilize the discharge.

The PDC electrodes were fabricated from pure tungsten weld rod of 0.04 in. dia. The collector anode was welded in the shape of a "T" which was then attached to a 12 in. long 1/8 in. dia. SS rod that passed through the vacuum seal and provided electrical connection. The PDC cathode was fabricated in a similar fashion absent the T assembly. The T-anode was positioned via a sliding seal and was made continuously rotatable to allow alignment with the axis of the electromagnet. This ensured field line alignment with the surface of the collector electrode. Teflon end caps were fitted to the T-anode ends to preclude electron collection on the butt ends of the anode rod where field lines intersected the collector. The end caps defined the active collection length of the anode as 1.5 cm and the active collection area as 4.79×10^{-5} m^2.

PDC anode magnetization was provided by a 4 in. dia. Helmholtz type electromagnet coil. The coil consisted of 360 turns of 18 gauge magnet wire wound on an aluminum spool. The spool was machined to allow water flow from a chiller at 4 – 20 °C and 15 lpm through the spool on the inboard side of the windings. The magnet coil was powered by an 80 V, 37 A (Sorensen DCS 80-37) DC power supply. The coil was indefinitely operated with a steady current of 5 A. The temperature measured by an imbedded K-type thermocouple was found to be less than 100 °C under these conditions. Magnetic induction as a function of coil current was measured to be ~67.7 G/A in air. Field uniformity was measured to be ± 1.5% at 10 mm from the axis along the center plane of the magnet.

A schematic of the microwave plasma experiment is shown in Fig. 2. This setup comprised a 1.5 kW maximum output power, 2.45 GHz microwave power unit and generator with circulator and dummy load (Applied Science and Technology, ASTEX-AX2100); three stub tuner (AX3041); and downstream plasma applicator (AX7610). The device was typically operated at 200 – 1000 W cw with ≤ 1% reflected power. Tap water at ~20 °C and 0.65 lpm was sufficient to cool the applicator to allow continuous operation at full rated power. A mass flow controller (MKS 1179A) provided steady, regulated He gas flow in the range 0 – 100 sccm. Device performance, however, was not found to be influenced by changes in the mass flow rate. A flow rate of 50 sccm was, therefore, used throughout since this choice proved convenient for pressure adjustment. Throttling the vacuum valve allowed adjustment of the He gas pressure in the range of 0.2 – 10 Torr for the experiments discussed here. A UV light "soft" initiator lamp was provided for breakdown initiation, but was not required in the discharges studied here.

The PDC electrodes employed in the gas discharge cell were replicated for use in the microwave system with the following exceptions: 1) the T-anode was changed to 0.094 in. dia. SS rod to increase the collection area to 1.125×10^{-4} m^2, and 2) the Teflon end caps were replaced with diamond-tool machined hard Alumina as it is well known that only W, SS, and Alumina are able to survive the high power plasma environment in the microwave system. The same electromagnet set was used in both systems. For the microwave system, the coil separation had to be increased from ~1.25 in. to 3 in. resulting in a reduction in the induction calibration to ~27.9 G/A in air.

A single-tipped Langmuir probe was employed to measure n and T_e in both experiments. The probe consisted of a 0.04 in. dia. W weld rod tip extending 5 mm beyond the end of a short section of Alumina 2-bore with 0.052 in. ID and 0.156 in. OD which was then telescoped inside a 12 in. long section of Alumina single bore, 0.188 in. ID and 0.25 in. OD. Using a separate 600 V, 2A DC power supply, the probe was biased over the current-voltage characteristic from full ion saturation to the exponential electron collection region. Probe bias was manually swept from 30 – 50 V below to several volts above the floating potential. The collisionless, thin-sheath model was employed for probe data analysis such that the probe current was related to the electron density, n, electron temperature, T_e, sheath thickness, x_s, and plasma potential, V_p, by

$$i_{probe} = en\sqrt{\frac{kT_e}{M}}A\left(1 + x_s/r_p\right)\left\{\frac{1}{2}\left(\frac{2M}{\pi m}\right)^{1/2}\exp\left[\frac{e}{kT_e}\left(V - V_p\right)\right] - \exp(-1/2)\right\}$$

where A is the probe surface area and r_p is the probe radius. The probe area correction $(1+x_s/r_p)$ allows for sheath expansion with increasing bias potential away from the plasma potential. A non-linear least squares filter based on the Levenberg-Marquardt algorithm was used to find the four free parameters sited above. Plasma parameters were found in the range 1 – 2 eV and $2.5 - 6.2\times10^{10}$ cm^{-3} in the glow discharge experiment, and 2 – 6.5 eV and $1 - 3.2\times10^{12}$ cm^{-3} in the microwave generated plasmas.

Results and Discussion

The results from PDC experiments in the glow discharge device are shown in Figs. 3 – 7. The nominal operating conditions for the glow discharge tube were ~100mA and ~350 V discharge current and potential, and 1 Torr He gas fill. In Fig. 3, both open circuit (V_o) and PDC (V_{PDC}) voltages are shown as a function of magnet coil current. The evaluation of Eq. 4 with kT_e~1.92 eV and Ω = 18.9 at I_B = 5 A (B = 350 G) is also shown for comparison. There is reasonable agreement here with the measured open circuit voltage. The PDC potential with the circuit loaded to 20 kΩ is also shown in Fig. 3. The loaded PDC voltage was found to be consistently ~ ½ V_o indicating that this load impedance was close to that of the PDC source for the conditions of this experiment.

Figures 4 and 5 summarize the PDC results obtained by varying the load resistance from 100 Ω to 10 MΩ. In Fig. 4, the PDC voltage was observed to increase steadily from the short circuit condition at $R_L \lesssim 1$ kΩ to voltages approaching the open circuit voltage (>6 V) at $R_L \gtrsim 1$ MΩ. The PDC current decrease was found to be consistent with the output voltage trend. The PDC extracted power to load R_L is shown in Fig. 5 as a function of load resistance (power-load curve). The power-load curve peaks at the impedance matched condition, ~20 kΩ, at a maximum extracted power of ~0.44 mW.

The results of varying the helium fill pressure and discharge current as potential routes to increase the extracted power are shown in Figs. 6 and 7, respectively. At the load matched condition, $R_L = R$, the peak extracted PDC power should be expected to behave as $(V_o)^2/R$. At constant B, ignoring the weak logarithmic dependence in the other contributors to Ω, and considering only electron-neutral collisions, the PDC power scaling predicts

$$P_{PDC} \sim \frac{n}{n_n} T_e^{3/2} \qquad - 6$$

where n_n is the neutral atom density in the discharge tube which is proportional to the gas fill pressure. Holding T_e constant, P_{PDC} can be expected to scale as

$$P_{PDC} \sim \frac{i_{discharge}}{p_{He}} \qquad - 7$$

where $i_{discharge}$ is the glow discharge current and p_{He} is the He gas pressure. P_{PDC} increased with increasing glow discharge current and decreasing He gas pressure according to Eq. 7 as shown in Figs. 6 and 7.

The observed PDC power scaling with discharge current and pressure in the discharge device suggests obvious paths to power scale-up through reduction in the neutral to charge density ratio and concomitant increase in the plasma conductivity. At similar He fill pressure (*i.e.* ~1 Torr), the microwave device operated at greatly increased charge density over that in the glow discharge experiment. Figure 8 shows the results of Langmuir probe electron density measurements in the microwave experiment at 1 Torr He as a function of microwave power density. The result was a density scale-up by almost two orders in magnitude over the glow experiment results.

Device and discharge conditions were compared for the two experiments in table 1. A direct application of Eq. 4 predicted an open circuit voltage scale up by ~33% in the microwave experiment. Figure 9 shows V_{PDC} and i as functions of load resistance for 1 Torr He microwave plasma at 8.55 W/cm^3 input power density. The asymptote in V_{PDC} is the open circuit voltage approaching 7.5 V, an increase of ~15.4% over that in the discharge experiment.

An estimate of the PDC power scale-up across two experiments is given by combining the predicted potential scaling (Eq. 4) with expected conductivity change based on electron-neutral collisions such that

$$\frac{P_{PDC_2}}{P_{PDC_1}} = \frac{V_{PDC_2}}{V_{PDC_1}}\frac{i_2}{i_1} = \left(\frac{V_{0_2}}{V_{0_1}}\right)^2 \frac{R_1}{R_2}$$
$$= \left(\frac{kT_{e_2}}{kT_{e_1}}\right)^{3/2}\left[\frac{\ln(1+\Omega_2^2)}{\ln(1+\Omega_1^2)}\right]^2 \frac{(A_p n)_2}{(A_p n)_1}\frac{n_{n_1}}{n_{n_2}} \qquad - 8$$

where subscripts 1 & 2 refer to differing devices or conditions, and A_p is the PDC electrode active collection area. Comparing the microwave device conditions with those in the glow discharge for the potential ratio found above and the device parameters found for 1 Torr He discharges in the respective devices enumerated in table 1, a PDC power scale-up factor of 158.4 was predicted.

PDC extracted power is shown in Fig. 10 as a function of R_L for the microwave discharge conditions of table 1. The optimal (impedance matched) condition in this case was near 600 Ω where the peak PDC power was 60 mW, a factor of 136.4 over that obtained in the glow discharge experiment.

Further improvement has been identified by varying the operating conditions slightly to 0.75 Torr He at 50 sccm. Figures 11 & 12 show V_{PDC} and P_{PDC}, respectively, as functions of the microwave power density for this pressure and 600 Ω load. This case demonstrated the maximum observed PDC performance. The PDC power increase to ~220 mW was consistent with a measured T_e increase to ~7 eV over the 1 Torr case (Eq. 4). Plasma density measured for this enhanced PDC performance case was similar to the 1 Torr case (Fig. 8). The asymptotic behavior in the PDC power with microwave power shown in Fig. 12 is consistent with the leveling off of the plasma conductivity suggested by the density roll-over in Fig. 8.

The conversion efficiency, ε, is estimated as the ratio of conversion to input power densities in the plasma discharge device

$$\varepsilon = \frac{p_{PDC}}{p} \qquad - 9$$

Here $p_{PDC} = P_{PDC}/V_{PDC}$, where V_{PDC} represents the plasma volume accessible to PDC power extraction, and p is the input power density to generate and sustain the discharge. (In a CA plasma, the external power input may be reduced substantially below that required in a non-CA plasma.) As the probe's electrostatic influence does not extend beyond the pre-sheath, the relevant interaction volume is defined by the electron mean free path for collisions in this high pressure discharge, and becomes an annular cylindrical volume surrounding the probe extending λ_{mfp} from the probe surface. By way of example for the microwave discharge experiment, at 1 Torr in He the electron λ_{mfp}

~0.082 cm. The PDC accessible plasma volume is then ~0.124 cm^3, making the collection power density ~1.61 W/cm^3 and the conversion efficiency ~18.8% for this case.

The V_o scaling with electron temperature (Eq. 4) indicates a strong T_e dependence in the conversion efficiency, (Eq. 9). Furthermore, the inverse dependence on plasma resistance $\left(\varepsilon \sim 1/R = A_p/\eta l\right)$ reflects positive probe area scaling and inverse plasma resistivity scaling, indicating clear directions for further performance improvement. Further optimization of PDC power conversion on a single electrode set is in progress as well as power scale-up with multiple electrode sets. A linear power scale-up is anticipated. It is, however, recognized that indefinite increase in electrode number and size relative to that of the discharge is not possible without interfering with plasma conditions. A more detailed efficiency analysis incorporating the affect of electrode perturbation on the plasma should be considered. Discharge seeding by CA-plasma catalysts such as certain alkali and alkali-earth metals [11] to increase charge density may also be employed in an effort to increase conductivity, extracted power, and efficiency, and may also lead to increases in the CA-plasma power.

Conclusions

Standard glow discharge and microwave plasma generation sources that provide reproducible, stable plasmas with power densities on the order of those of CA-plasmas were used to characterize plasmadynamic power conversion. The PDC generation of electrical power was experimentally demonstrated at the ~ ¼ W level in laboratory plasma devices for the first time. Glow discharge and microwave plasma sources were operated at power levels up to 50 W and 11.97 W/cm^3, respectively. In a glow discharge of 1 Torr He fill with T_e~1.9 eV and n~2.8×10^{10} cm^{-3}, PDC open circuit voltages were shown to increase with applied field strength (0-350 G) up to 6.5 V. These results were demonstrated to be in reasonable agreement with a simple model describing electron current retardation to a magnetized electrode. Power-load curves identify the impedance matching condition at 20 kΩ, for which the peak PDC extracted power is 0.44 mW.

Electron and neutral particle density scaling experiments for P_{PDC} reveal the strong dependence on plasma conductivity. Power scale-up was demonstrated in a microwave device which generated plasmas in 1 Torr He with T_e~3.7 eV and n~3.2×10^{12} cm^{-3}. The charge density, electron temperature, and electrode collection area scale-up were the dominant affects in a PDC power scale-up by a factor of almost 140 over the glow discharge PDC results. PDC extracted power to 60 mW was found in a 1 Torr He microwave discharge at 8.55 W/cm^3 and 600 Ω load match. The reduced load match was itself evidence of a greatly enhanced plasma conductivity. P_{PDC} to ~200 mW was found in the microwave experiment at 8.55 W/cm^3 and 0.75 Torr He. Peak output performance to 220 mW PDC power was obtained at 11.97 W/cm^3 microwave input.

Plasmadynamic conversion may be optimized for high power and efficiency. The system is simple with projected costs on the order of 1% those of fuel cells. The implications for microdistributed power are profound. Scale-up to several to 10s of W in a small, modular array converter unit is under development. Autonomous, chemically driven, power producing plasma units outfitted with plasmadynamic collection devices are envisioned which could enable microdistributed electrical and motive power applications without infrastructure requirements other than those of its manufacture and distribution.

Acknowledgements

The authors would like to thank Dr. M. Nansteel for many useful discussions and excellent technical assistance during the experimental phase of this effort.

References

[1] R. G. Mills, *Nuclear Fusion*, **7**(1967)223.

[2] D. L. Rose, *Nuclear Fusion*, **9**(1969)183.

[3] G. H. Miley, *Fusion Energy Conversion*, American Nuclear Society, La Grange, IL, 1976.

[4] R. Mills, N. Greenig, S. Hicks, Int. J. Hydrogen Energy, **27**(2002)651.

[5] R. Mills, M. Nansteel, and Y. Lu, Int. J. Hydrogen Energy, **26** (2001) 309.

[6] R. L. Mills and P. Ray, *New J. Phys.*, **4** (2002) 22.1.

[7] R. M. Mayo, R. L. Mills, and M. Nansteel, *On the Potential for Direct or MHD Conversion of Power from a Novel Plasma Source to Electricity for Microdistributed Power Applications*, IEEE Transactions on Plasma Science, 2001, in press.

[8] I. Alexeff and D. W. Jones, *Phys. Rev. Lett.*, **15**(1965)286.

[9] F. F. Chen, *Electric Probes*, in *Plasma Diagnostic Techniques*, R. H. Huddlestone and S. L. Leonard, eds., Academic Press, NY, 1965.

[10] D. Bradley, S. M. A. Ibrahim, and C. G. W. Sheppard, Fourteenth Symposium (International) on Combustion, The Combustion Institute, Pittsburgh, 1973, p.383.

[11] R. L. Mills, J. Dong, and Y. Lu, Int. J. Hydrogen Energy, **25** (2000) 919.

Table 1: Device and discharge conditions for 1 Torr He.

Parameter	Glow Discharge Experiment	Microwave Experiment
A_p (m^2)	4.79×10^{-5}	1.125×10^{-4}
V_{PDC} (V)	6.5	7.5
n (cm^{-3})	5×10^{10}	3×10^{12}
n_n (cm^{-3})	3×10^{16}	3×10^{16}
T_e (eV)	1.5	3.7
Ω	18.9	4.8

Figures

Fig. 1 Schematic of the 1 in. glow type discharge tube and PDC electrode assembly. The outer ¼ in disk electrodes are the glow discharge electrodes. The magnetized PDC electrode is shown as the collector electrode. The unmagnetized PDC electrode is shown inside the alumina tube.

Fig. 2 Schematic of the microwave discharge experiment apparatus. Symbol definitions are as follows: P – pressure gauge, B – Baratron pressure gauge, MFC – mass flow controller, TC-K – type-K thermocouple, DC UV – DC power supply for the UV "soft" initiator. The PDC electrodes and magnet coil are not shown.

Fig. 3 Open circuit (○) and 20 kΩ PDC (△) voltages in the glow discharge experiment as a function of magnet coil current (67.7 G/A). Nominal operating conditions were 100 mA and 350 V discharge current and voltage. The dotted line shows the predicted open circuit voltage from Eq. 4.

Fig. 4 PDC extracted voltage (□) and current (○) for load resistances from 100 Ω to 10 MΩ in the glow discharge experiment in 1 Torr He and $I_B = 5$ A.

Fig. 5 PDC extracted power as a function of load resistance in the glow discharge experiment in 1 Torr He and $I_B = 5$ A.

Fig. 6 PDC extracted power as a function of He gas fill pressure in the glow discharge experiment at $R_L = 20$ kΩ and $I_B = 5$ A.

Fig. 7 PDC extracted power as a function of discharge current in the glow discharge experiment at 1 Torr He and $I_B = 5$ A.

Fig. 8 Langmuir probe measurements of electron density in the microwave experiment as a function of microwave power density for 1 Torr He at 50 sccm.

Fig. 9 PDC voltage (□) and current (○) as a function of load resistance in the microwave device at 8.55 W/cm^3, and 1 Torr He at 50 sccm.

Fig. 10 PDC extracted power as a function of load resistance in the microwave device at 8.55 W/cm^3, and 1 Torr He at 50 sccm.

Fig. 11 PDC potential as a function of microwave power density for $R_L = 600$ Ω, and 0.75 Torr He at 50 sccm.

Fig. 12 PDC extracted power as a function of microwave power density for $R_L = 600$ Ω, and 0.75 Torr He at 50 sccm.

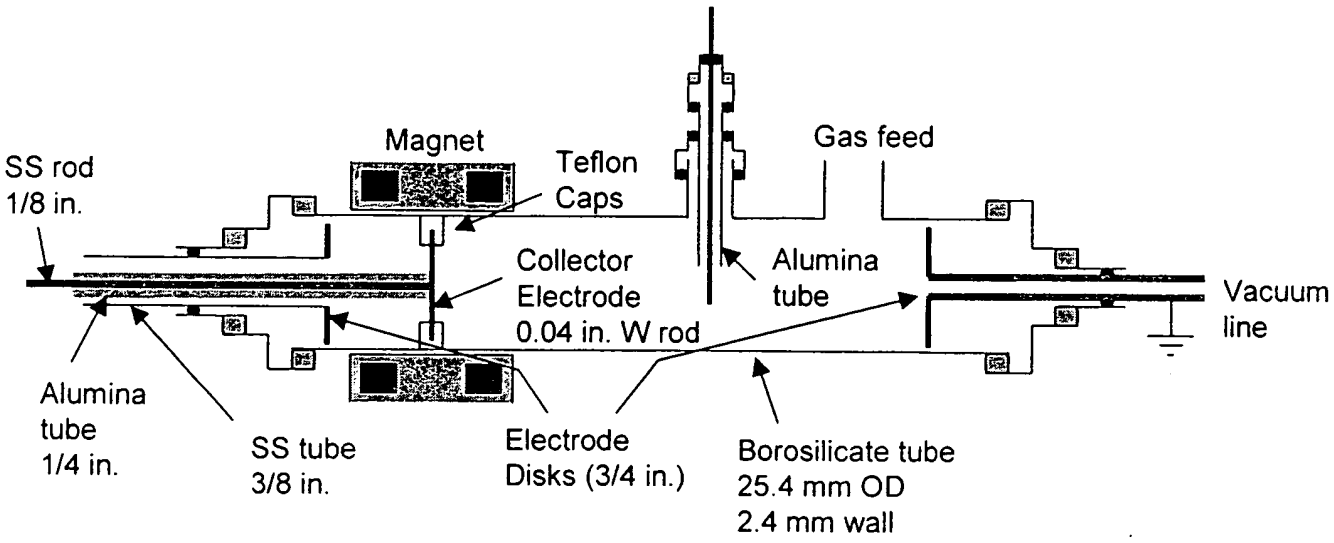
SS rod
1/8 in.
Magnet
Teflon
Caps
Gas feed
Collector
Electrode
0.04 in. W rod
Alumina
tube
Vacuum
line
Alumina
tube
1/4 in.
SS tube
3/8 in.
Electrode
Disks (3/4 in.)
Borosilicate tube
25.4 mm OD
2.4 mm wall

Figure 1

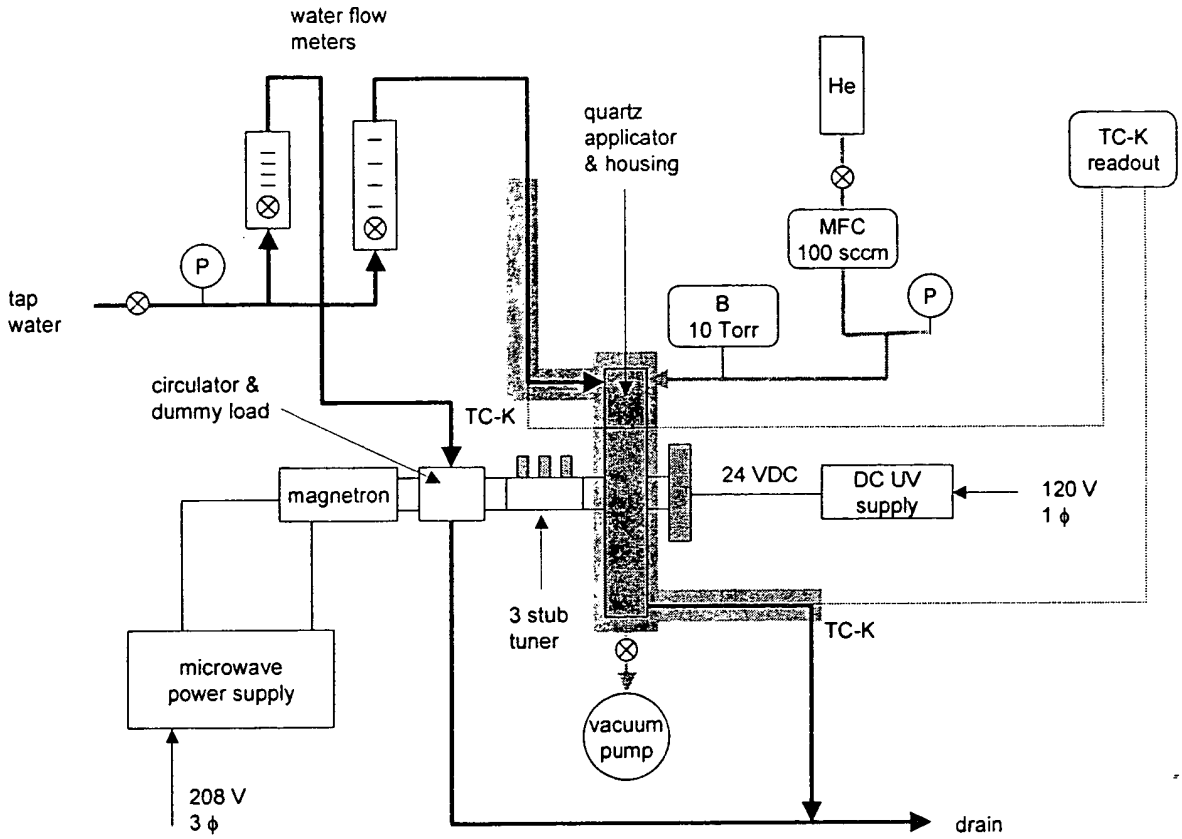
water flow
meters
He
quartz
applicator
& housing
TC-K
readout
MFC
100 sccm
P
tap
water
P
B
10 Torr
circulator &
dummy load
TC-K
magnetron
24 VDC
DC UV
supply
120 V
1 ϕ
3 stub
tuner
TC-K
microwave
power supply
vacuum
pump
208 V
3 ϕ
drain

Figure 2

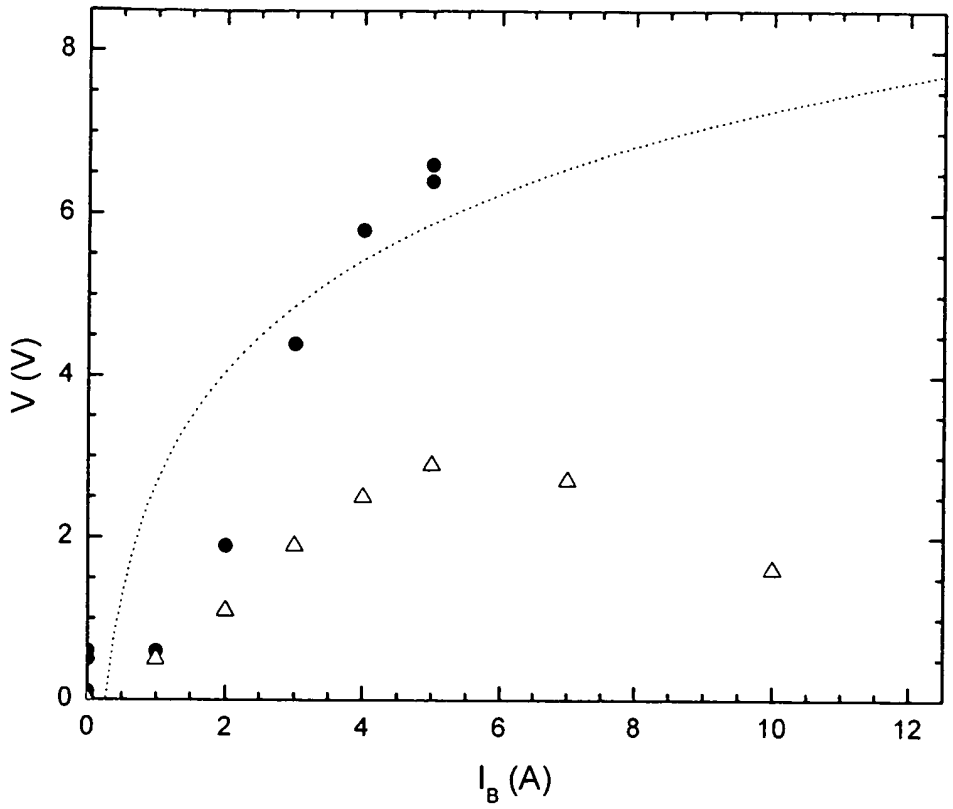

Figure 3

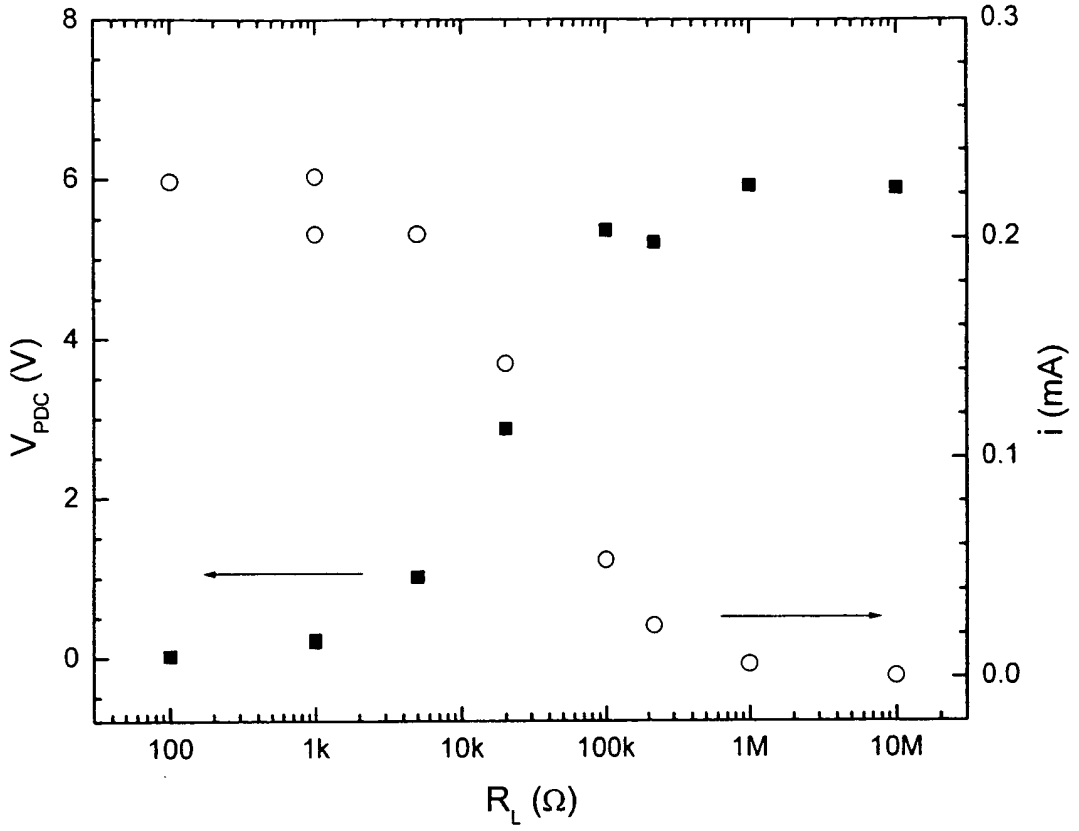

Figure 4

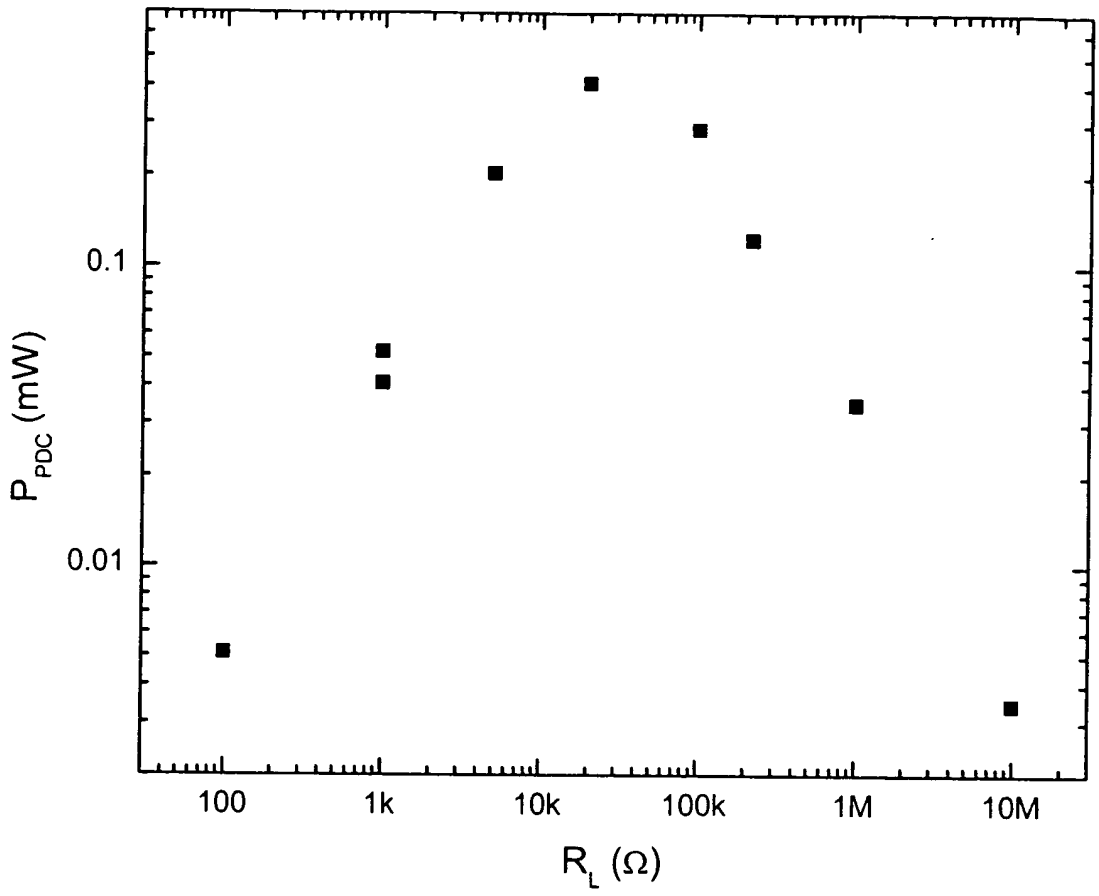

Figure 5

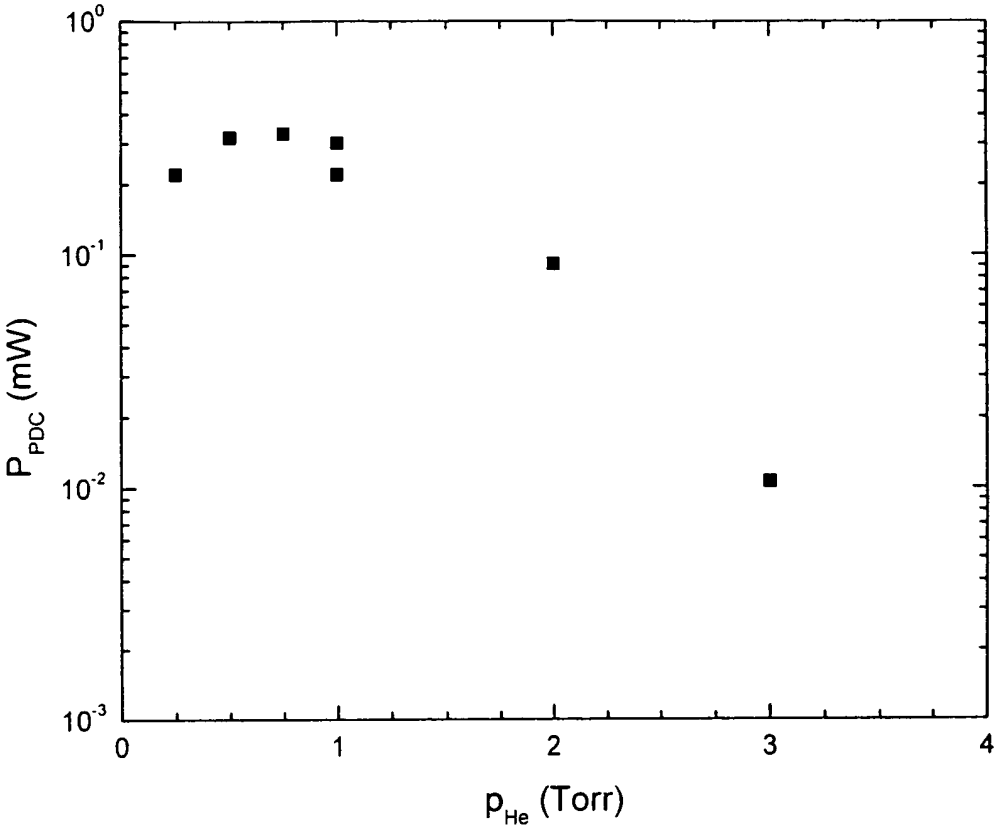

Figure 6

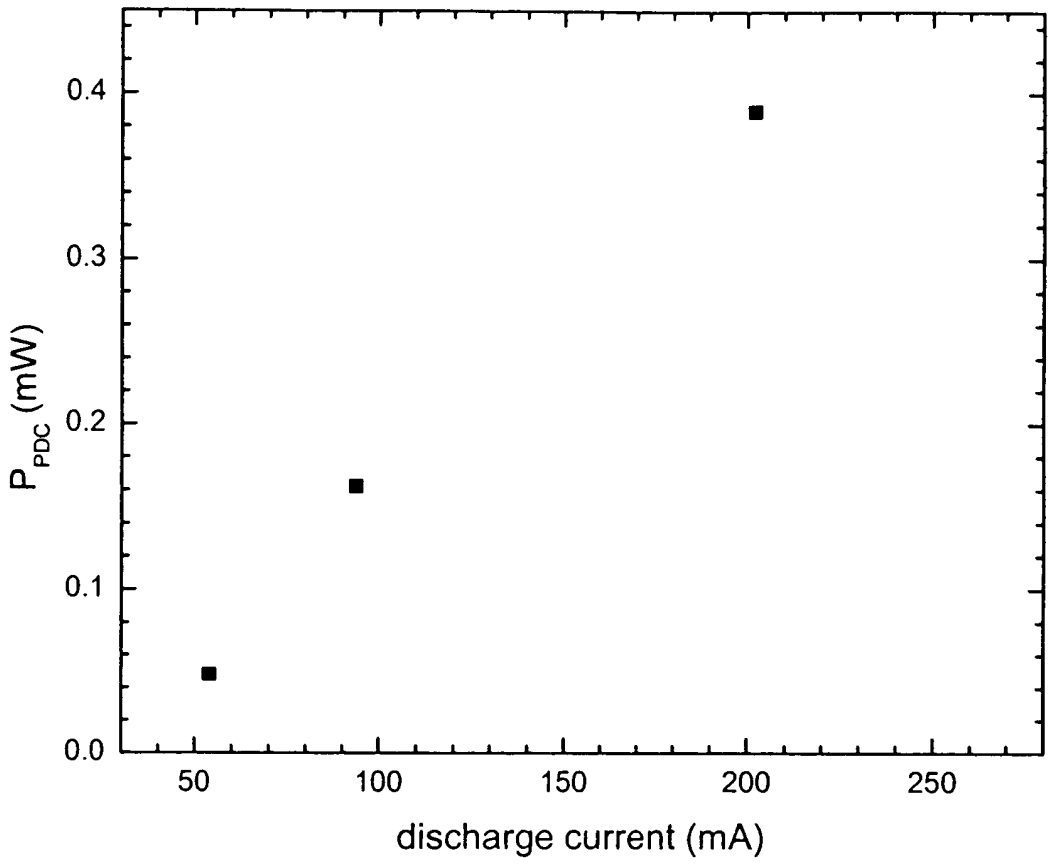

Figure 7

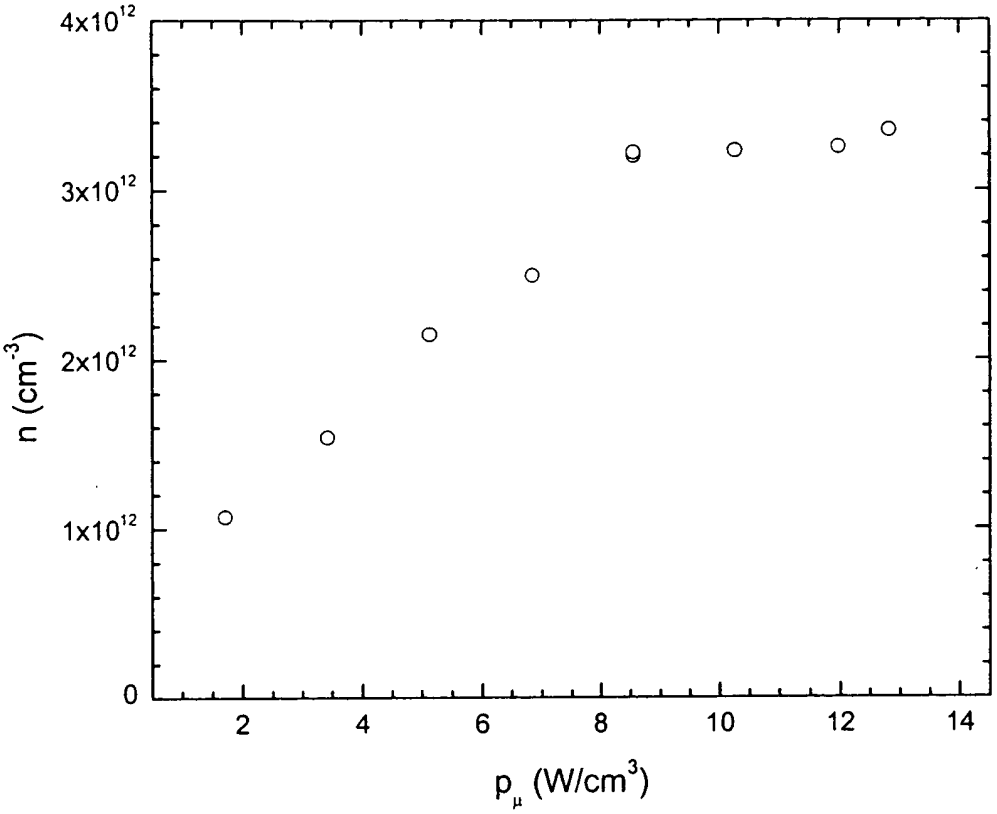

Figure 8

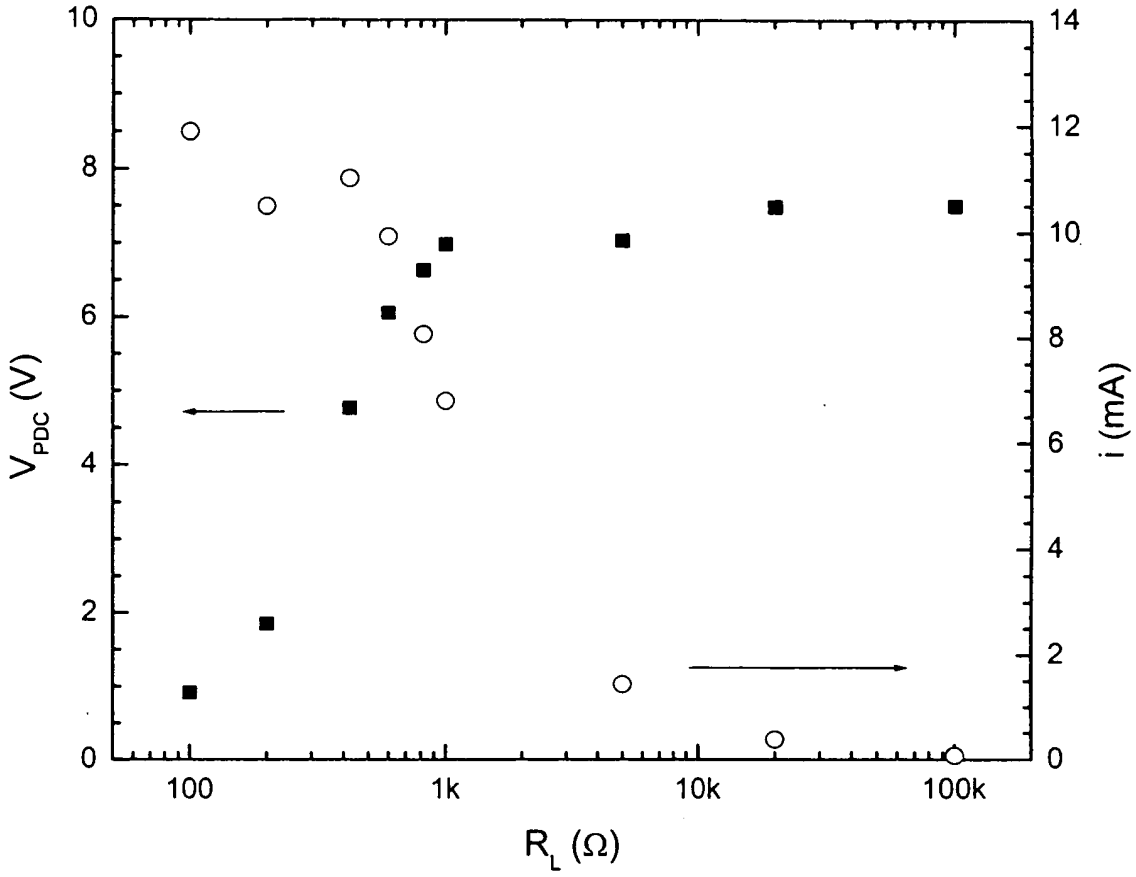

Figure 9

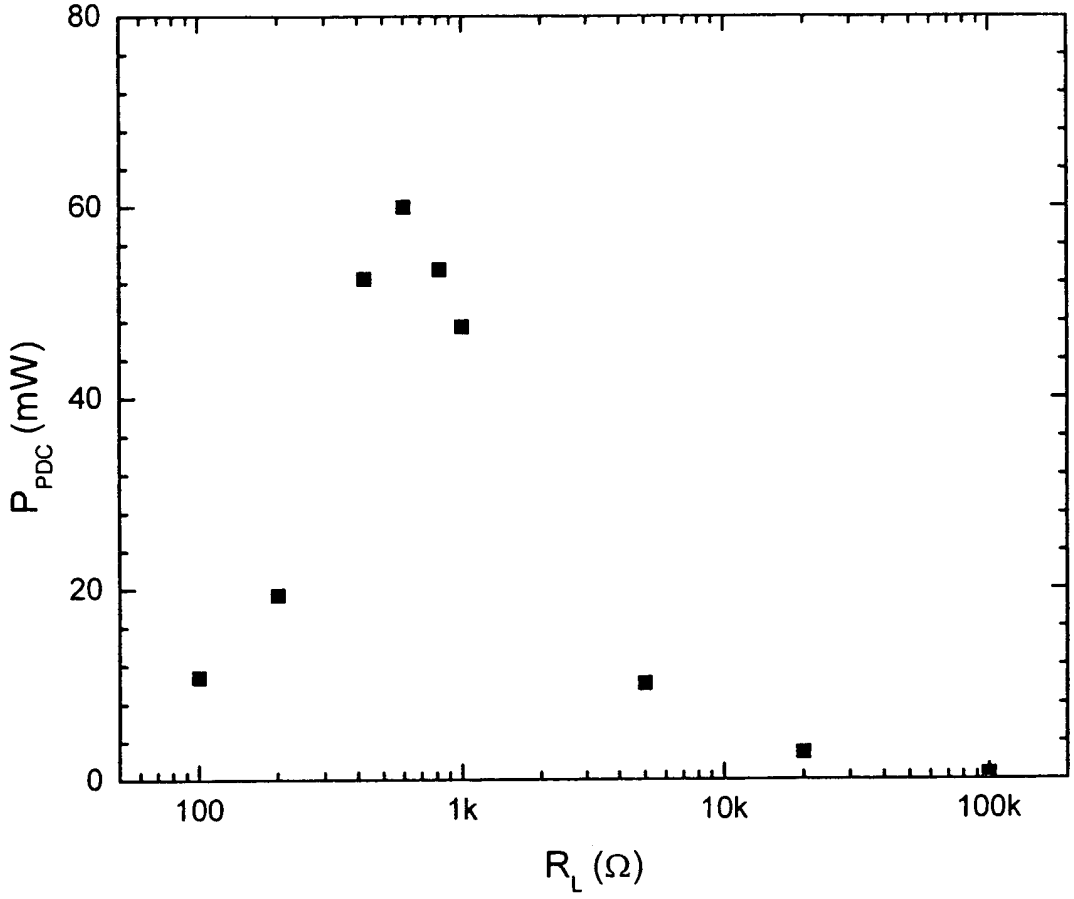

Figure 10

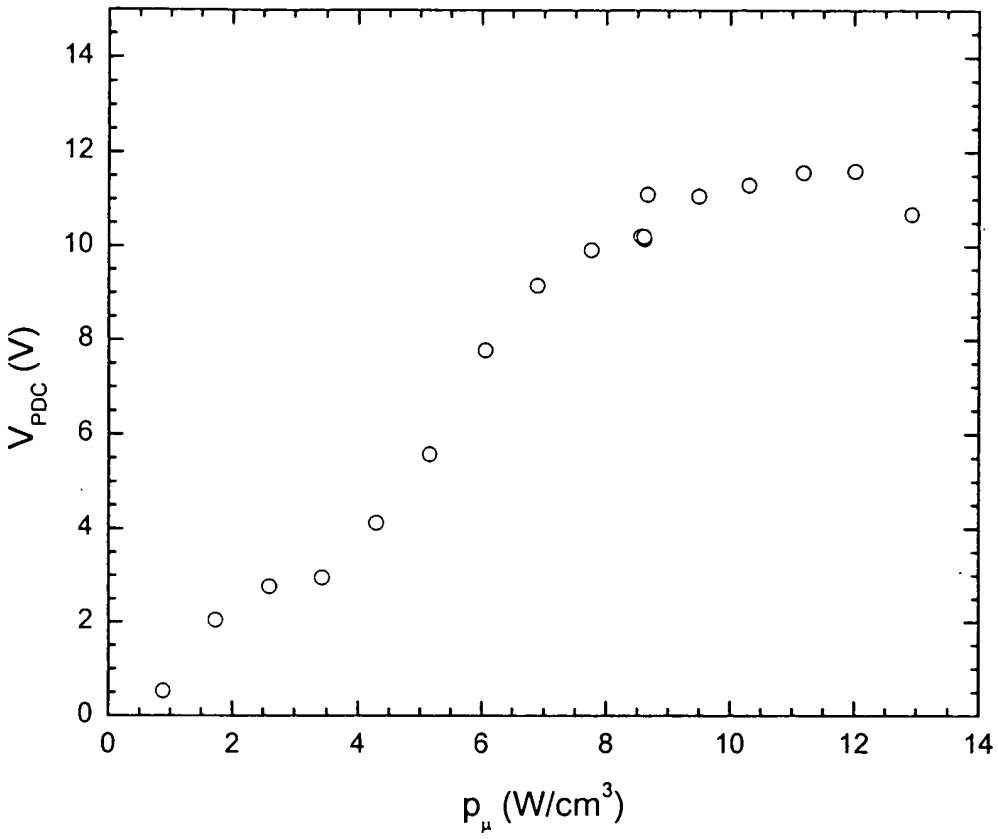

Figure 11

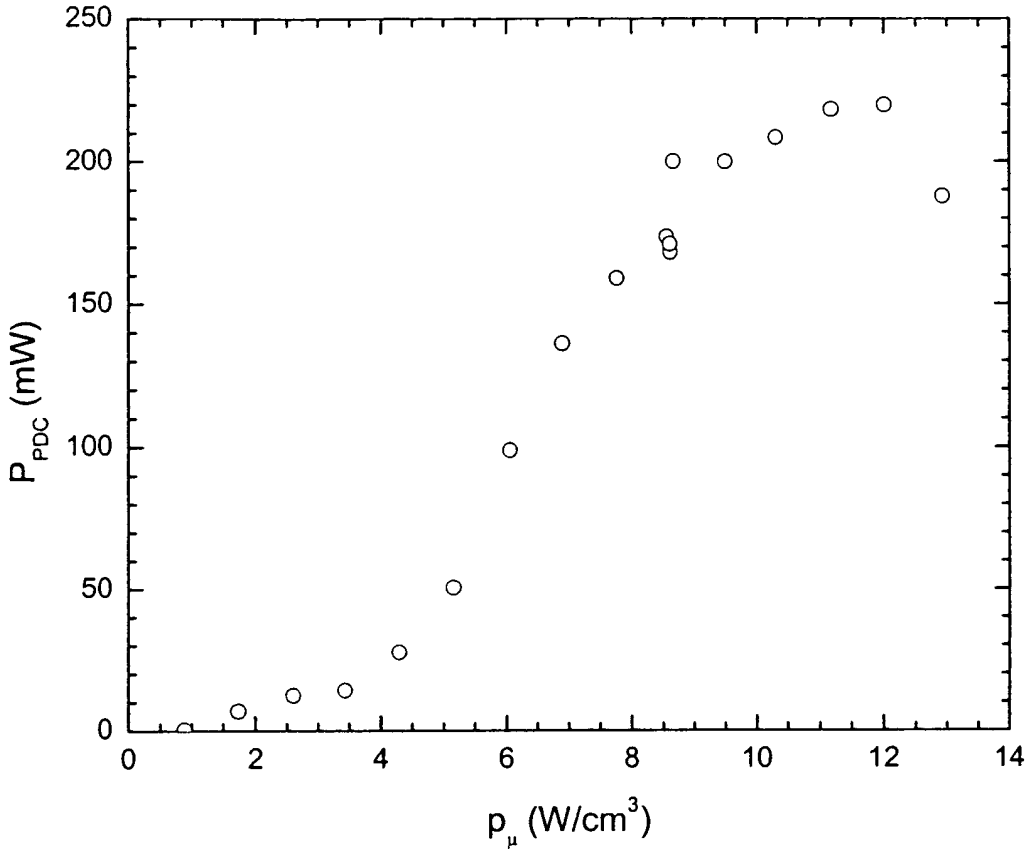

Figure 12

Emission in the Deep Vacuum Ultraviolet from an Incandescently Driven Plasma in a Potassium Carbonate Cell

H. Conrads*, R. Mills**, Th. Wrubel***

* Wolfshovener Strasse 195, 52428 Jülich, Germany

** Black Light Power, Inc., 493 Old Trenton Rd., Cranbury, N.J. 08512, USA

*** Institute for Experimental Physics V, Ruhr University, 44780 Bochum, Germany

Abstract

Electromagnetic radiation in both the visible and vacuum ultraviolet (VUV) spectral ranges was emitted from an incandescently driven plasma in a potassium carbonate cell after the potassium carbonate coated on a titanium mesh was heated to above 750°C in a hydrogen atmosphere. The pressure was between 0.1 and 1 mbar, and the hydrogen was dissociated by a hot tungsten wire. Bright visible light filled the annulus between the coaxial tungsten heater and the titanium mesh. This grid was at a floating potential. The emission of the H_α and H_β transitions as well as the L_α and L_β transitions were recorded and analyzed. In the latter spectral range, the spectra show rotational-vibrational transitions of molecular hydrogen which belong to the Werner-band-system of molecular hydrogen. The plasma generated in the incandescently driven cell has phenomenological similarities to that of low pressure electrical driven discharges such as striations of the plasma or the appearance of unipolar arcs ending on metal surfaces. However, the plasma seemed to be far from thermal equilibrium and dependent on the chemistry of atomic hydrogen with potassium. Details of the chemistry powering a novel VUV-light source could not be revealed within the frame of this contribution.

I. Introduction

Table top sources emitting radiation in the deep ultraviolet spectral range are gaining more and more interest in photochemistry due to the increased functionalization of surfaces, particularly in combination with lithographic processes [1]. The range and complexity of applications are wide and range from simple sterilization of large surfaces to sophisticated nano-patterning in production processes of microelectronics and biotechnology [2]. Well known sources such as electric sparks [3], capillary discharges [4], pseudosparks, hollow cathode discharges [5], laser sparks, and barrier discharges [6], to name a few, are suited for

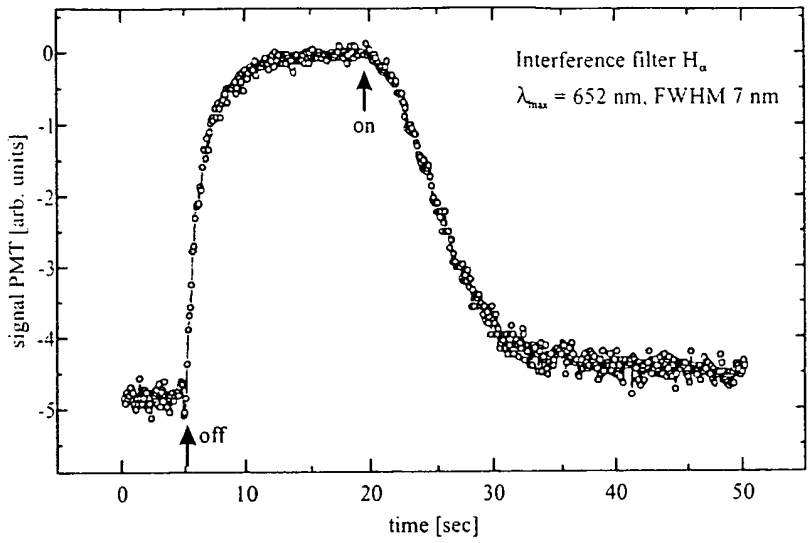

Figure 1: Emission of the cell as a function of time, while the heater current was turned of and on.

such photochemical work and are selected and developed further according to the specifications of the particular application.

Previously reported VUV emission of incandescently driven potassium carbonate cells in hydrogen [7] seemed to depend more on the chemistry of the potassium with hydrogen—with sodium carbonate no VUV emission was observed—and on the temperature of components in the cell than on a particular voltage or current applied to the cell. Figure 1 shows the decay and return of the H_α emission, which is indicative of an associated VUV emission, when the power was turned off and on in several ms. After turning off the heater power, the intensity dropped with a time constant of 2 seconds. With restoration of the original heater power, 10 seconds elapsed before the H_α emission reached its maximum again.

The following paper addresses the plasma and the VUV radiation generated in such a cell. The emission of the first two members of the Balmer and Lyman series were recorded with higher spectral resolution than before [7], and in contrast to earlier investigations, the tungsten wire was heated by external radiation as well as by ohmic heating.

II. Experimental set up

A. The Cell

Three different types of cells were used to investigate the formation of a low-voltage hydrogen plasma and the emitted radiation. One design, type I, was described previously [8]. In the second design, type II, the helical tungsten wire heater was replaced by two commercial 120 V halide bulbs connected in parallel. A tungsten wire was wrapped around the outside of the bulbs to serve as a hydrogen dissociator [9]. The tungsten wire in the type II cell as well as the titanium mesh were at a floating potential. All other components were the same as those of the type I cell. In the third design, type III, the thermal insulation of the quartz tube vacuum vessel of the type I cell was removed and replaced by an oven. An adjacent part of the tube had no insulation in order to allow for "side on" observation of the radiation. The rest of the quartz tube was covered by a brass tube that extended to the cap which provided the different supplies. The voltage supplied to the tungsten wire heater was increased step-wise from 20 V to 70 V. At 70 V, the color of the tungsten wire was similar to the one in the center of the oven.

For the Lyman series measurements, all of the cells were windowless and connected to a VUV spectrometer directly for "end-on" observation. The visible radiation was coupled to the spectrometer by glass fibers for "side-on" observation.

B. The Spectrometers

The light in the visible spectral range was analyzed by a grating spectrometer in Czerny-Turner mounting and recorded by a photomultiplier and oscilloscope as well as by an optical multichannel analyzer (OMA) system. A 1200 lines/mm grating blazed at 1000 nm was used. The light in the vacuum ultraviolet was analyzed by a scanning 1 meter grating spectrometer in Eagle mounting (McPherson, model 225) equipped with a grating of 1200 lines/mm blazed at 120 nm. The spectra were detected by a photomultiplier coated by a p-Terphenyl scintillator and recorded by an oscilloscope. The entrance and exit slits had a width of 50 μm. A pressure gradient was maintained between the cell and the pumped spectrometer.

III. Experimental Results

A. The Cell

The work was started with a type I cell. As soon as the temperature between the quartz wall and the thermal insulation of the cell exceeded 700°C, light was observed from the annulus between the helical tungsten heater and the titanium mesh coated with a thin film of potassium carbonate. The temperature outside of the quartz tube was increased to and held constant at 750°C. The bluish-white-colored emission that lasted for about one hour increased with temperature and was brighter than the glow of the tungsten heater. The experiment was repeated several times until the tungsten heater wire became brittle.

Rather than replace the tungsten wire, a series of experiments was performed next using the type II cell. With an electrically floating tungsten wire wrapped around the outside of the bulbs, the light in the annulus became bright after 10 minutes of heating and was observed to be different in color compared to the bright light emitted from the interior of the bulbs. The bluish-white light was easily observed by eye. The cell wall temperature was again 750°C. The light emission lasted about half an hour. Without the tungsten wire wrapped around the halide bulbs, no bluish-white light emission was observed.

No significant difference in the spectral emission or general performance could be determined between the type I and type II cells. Furthermore, the endurance of the bulbs in type II cell was not significantly better than that of the tungsten heater of the type I cell due to failure of the quartz walls of the bulbs under the resulting high-temperature conditions. The quartz of the bulbs developed plasticity with loss of mechanical stability above 1000°C. This behavior was not observed when the external tungsten wire was absent corresponding to the absence of the generation of the bluish-white light emission from the annulus. Since the operative temperature at the quartz wall of the type II cell was 750°C as well, it was concluded that an exothermic reaction was responsible for the generation of light in the annulus that also required the tungsten to be at a sufficiently high temperature and the presence of potassium carbonate on the titanium mesh.

Next a type III cell was studied. When a current was passed through the tungsten heater of a type III cell, a zone of about 5 – 10 windings was observed to have a significant lower temperature than the other windings as indicated by a difference in color. This cooler zone slowly migrated back and forth along the heater axis. Often several of these lower temperature

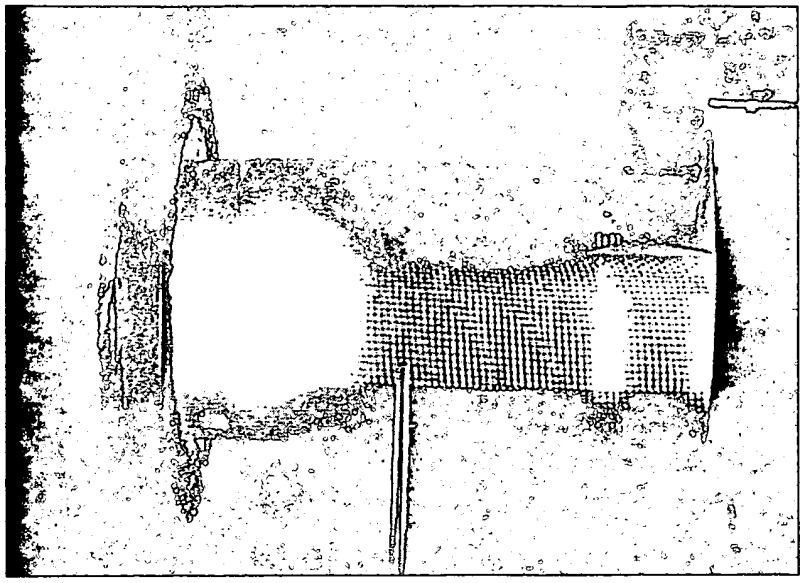

Figure 2: Photograph of the cell (type III). Bluish-white light can be seen at positions up to a few centimeters outside the oven (left) and the brass insulator.

zones were observed. A reasonable explanation for this phenomenon was that an electrical short formed across the zone of the darker windings due to a plasma created around the coil before the bluish emission in the annulus between the tungsten wire and the titanium grid could be visually observed. For the section of the heater that was observable, the voltage across the tungsten windings from one end of the cooler zone to the other was not more than 5 V. The emission of the tungsten wire and the associated voltage inside the insulating brass tube and the oven may have been different.

This segmentation of emission of the tungsten coil also remained active at a later stage when the light emission of the cell was fully developed as evident by the emission of the Balmer series of hydrogen. Then a greenish seam appeared around the dark zone directly pointing to an electrical short by a plasma. At this finally developed stage of the discharge, the bright zones of the tungsten wire shown in Figure 2 pointed to zones of higher axial electric fields. From the inhomogeneous light emission of the tungsten wire, it was concluded that an axial inhomogeneous field was generated in the annulus between the tungsten wire and the titanium mesh.

As shown in Figure 2, bluish light was emitted from the region between the titanium mesh and the quartz wall as well as from the annulus between the tungsten coil and the titanium mesh. A similar pattern was observed for the emission of white light. It was observed that a necessary

condition for this kind of emission was the existence of sufficient potassium carbonate on the titanium mesh, and the intensity of the bluish and white emission was related to the potassium carbonate concentration on the titanium mesh. In addition, it became evident that the temperature of the titanium mesh had to be sufficiently high to enable the emission. This was demonstrated by removing the oven and setting the tungsten coil at the rated voltage of 70 V for a time longer than that required to achieve strong emission. Only the red emission of the tungsten wire was observed. As soon as the oven was slipped over the quartz tube, the bluish and white emission started instantly.

Since the oven heating was sufficient to maintain the temperature of the titanium mesh sufficiently high for emission, the tungsten-coil heater power was reduced by decreasing its voltage. It was possible to sustain VUV light emission down to 20 V corresponding to about 0.2 V per winding and a field of about 0.1 V/cm. The light emission stopped with a voltage just below 20 V and returned at once when the voltage was restored to 20 V. When the voltage was set to zero for a while, the return of the light emission was delayed even when the voltage was quickly increased to 70 V. From these observations, it was concluded that the condition of a minimum tungsten-wire temperature was required in order to trigger the bluish and white light emission, when all of the other conditions were fulfilled. From the experiments with the light bulbs as heaters together with these findings, it was concluded that axial electric fields might be essential for the build up of the plasma and light emission, but an appropriately elevated temperature of the tungsten wire was necessary as well.

Radial plasma striations in the zones of bluish emission (see Figure 2) point to the existence of radial electric fields which might be generated due to chemical potentials in the vicinity of the titanium mesh or due to a Nernst potential because of a strong temperature gradient.

When the pressure in the quartz tube was raised to a couple of mbar, unipolar arcs developed on the titanium mesh. The dependence of this phenomenon on the voltage applied to the tungsten coil was similar to the case described above.

Striations of electric fields and their impact on electron properties in periodic states inside the plasma of a DC-glow-discharge have been analyzed in depth in references [10] and [11]. Since the observed space-resolved visible emission of the AC-driven cell is not very different from that in zones of DC glow discharges, it was concluded that the development of local electric field modulations and distinct non local electron properties may govern this kind of plasma as well. Dark zones in the annulus between tungsten coil and titanium mesh as well as outside the titanium mesh may have been zones of acceleration of free electrons. Electrons

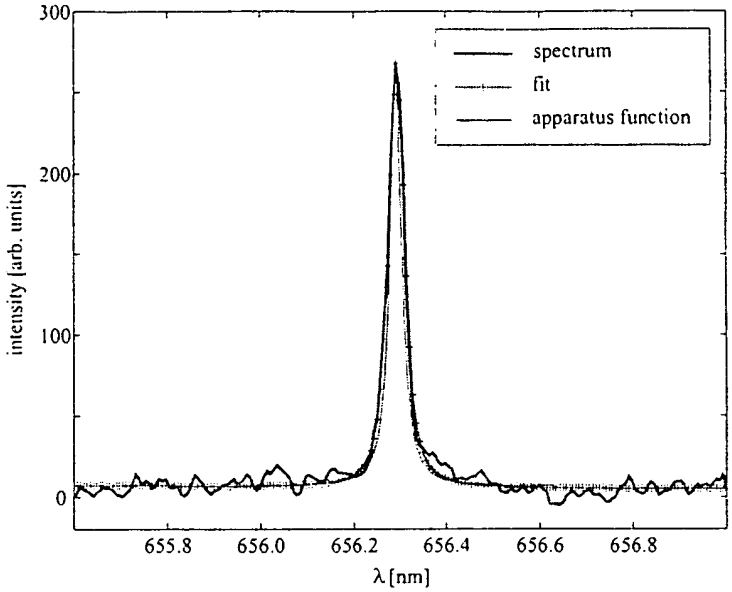

Figure 3: The emission of the H_α measured in second order together with it best fit and the apparatus function.

may have been accelerated axially and/or radially depending on the site in the cell. Inside the bright zones of the plasma the electrons may have lost a part of their energy due to interaction with heavy particles. A local pattern of the velocity distribution of the electrons in periodic states depends on partial pressures of the constituents and the local field distribution [10,11]. Both of these parameters could not be controlled during the reported experiments. It is therefore not too surprising, that the spectral emission such as that in the VUV varied between the different experimental runs as shown in Figures 4a and 4b. The plasma generated by the cell seems to be complex and requires further investigations. These issues are discussed in Sec. IV.

B. The Spectra

For the investigation in the visible spectral range, the wavelength was calibrated using a cold standard lamp that also served for the determination of the apparatus function which was fit by a Voigt profile of 0.96 pixels Gaussian and 3.89 pixels Lorentzian widths. In the first order, the width of the H_α transition ($\lambda = 656.28\,nm$) corresponds to that of the apparatus profile; whereas, in the second order, a broader and slightly asymmetric H_α profile was observed. Figure 3 shows the emission of the H_α transition measured in the second order with

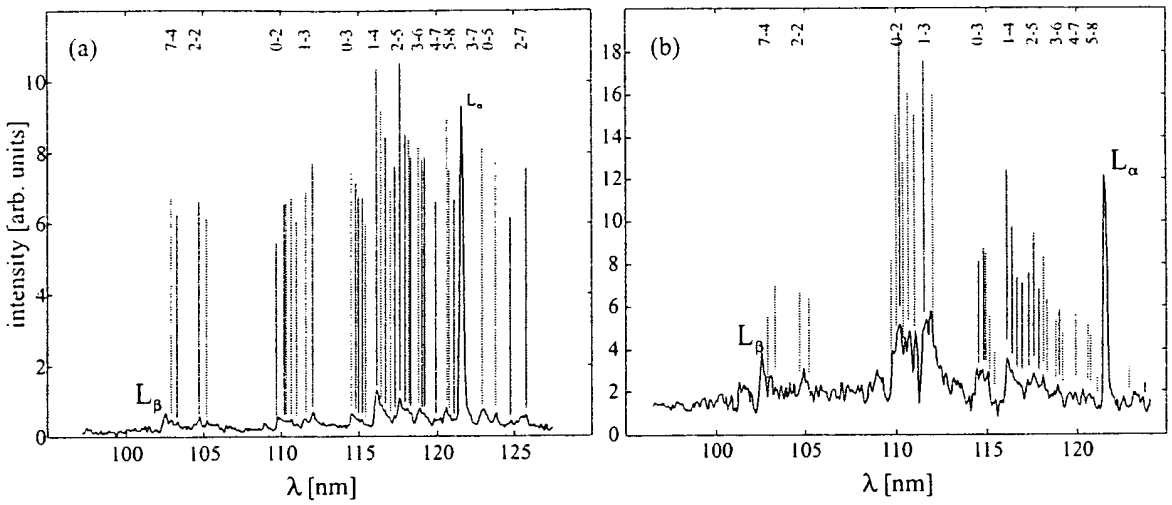

Figure 4: Examples of spectra of the L_α and L_β transitions showing rotational-vibrational transitions belonging to the Werner band system.

a reciprocal dispersion of 7.0 pm/channel together with a least squares fit. The calculated profile consists of three wavelength shifted Gaussian profiles according to the three fine structure transitions of H_α taking into account the intensity ratios given by [12]. The calculated profile is still asymmetric when it is convoluted with the measured apparatus function. Therefore, the asymmetry on the measured spectra can be attributed to the unresolved observation of the fine structure components. The fit gave a Gaussian width of (3.2 +/- 0.9) pixels corresponding to (22 +/- 0.06) pm. This served for an estimation of an upper limit of the ion temperature of $k_B T_e = (0.1 - 0.32)\ eV$.

The H_β transition was identified in the spectra measured in first order. It was not observed in second order because of its low intensity. The intensity ratio of the H_α and H_β transitions was determined to be 15 +/- 5 with a relatively high uncertainty due to the low intensity to noise ratio of the H_β transition. By assuming a Maxwell Boltzmann distribution of the level population, an electron temperature of $k_B T_e = (0.30 - 0.43)\ eV$ was deduced. Since the electron density of the present plasma was small, the assumption of a Maxwell distribution was somewhat questionable. Nevertheless, only a slightly higher temperature of $k_B T_e = (0.32 - 0.48)\ eV$ was found when a corona model was applied. In both cases, radiation transport was neglected in the calculations so that the temperature given represents an upper limit.

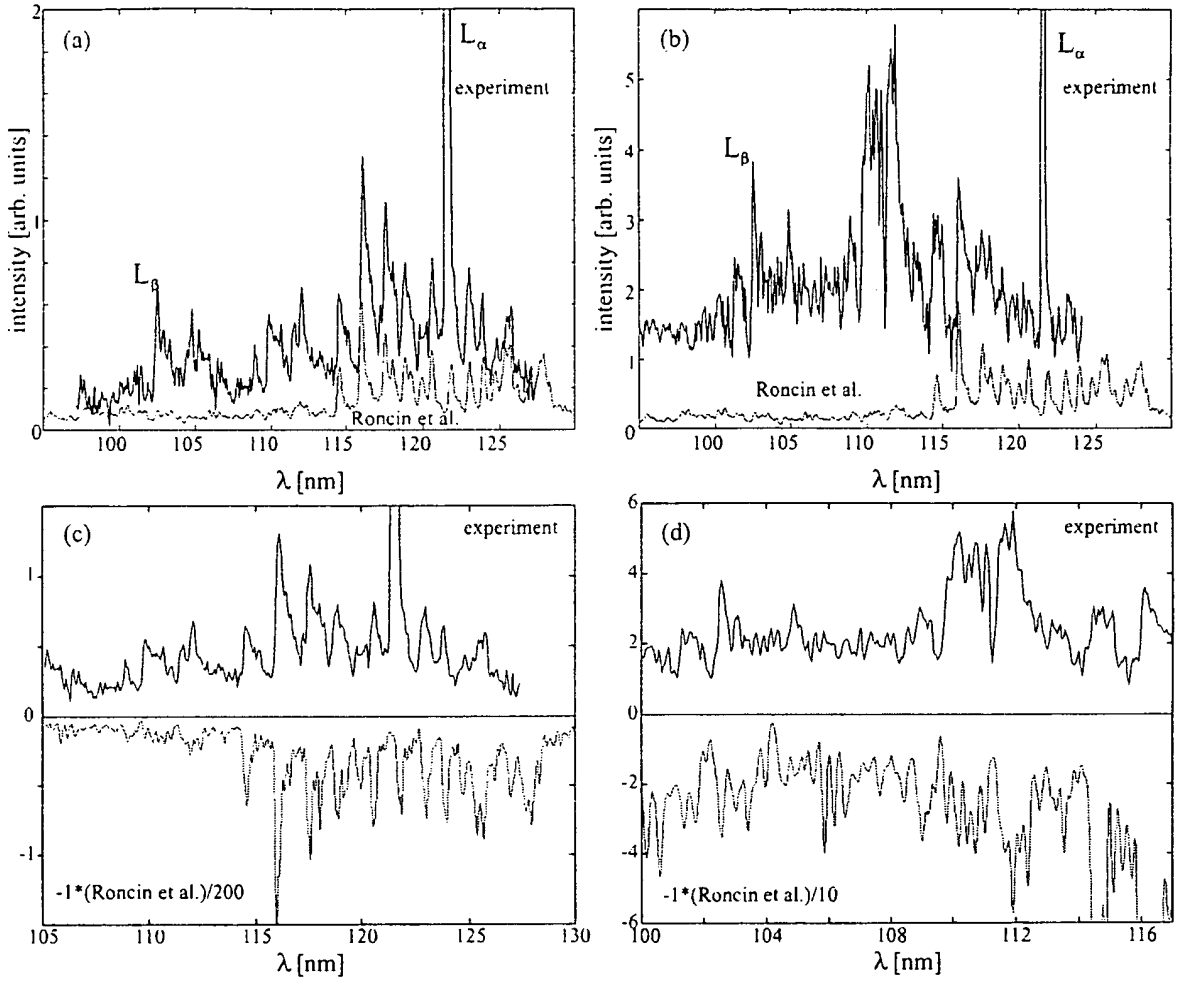

Figure 5: The measured spectra in comparison with a synthetic emission spectrum (intensity-scaled) of molecular hydrogen after /14/. a,c) and b,d) correspond to the experimental spectra in Figure 4a) and 4b), respectively.

Figure 4 shows two scanned spectra in the vacuum ultraviolet spectral range where the emission of the L_α and L_β can easily be seen. Strong emission of bands and lines were also observed in this wavelength region which will be discussed later. The intensity ratio of the L_α and L_β transitions was measured with a higher accuracy to be 16.5. For an optically thin plasma, the corresponding temperature of a Boltzmann level population is 62 eV. This excessive energy may indicate that this model is not applicable possibly because of the large distance of the energy levels. For these series transitions to the ground state, a corona model may be more suitable which gave an upper estimate of the electron temperature of

$k_B T_e = 1.6\ eV$. Nevertheless, this temperature was also factors higher than the above estimated temperatures indicating that at least the emission of the L_α may have suffered from radiation transport.

In summary, the data indicate that the electron temperature of the present plasma was not higher than $k_B T_e = 0.5\ eV$. On this basis, it was astonishing that the Lyman alpha and Lyman beta transitions appeared in the spectra since an excitation energy of 10.2 eV and 12.1 eV is required, respectively. The same holds for the Balmer series as well. The Lyman-α energy is a factor of about 20 above the measured thermal energy. The amount of electrons in the Maxwell tail that had enough energy to enhance the Lyman transition was 11 orders of magnitude lower than the total number of electrons.

Figure 5 shows the spectra of Figure 4 together with an emission spectrum of the Werner bands of the hydrogen molecules taken from reference [13]. The experimental spectra in this reference have a coincidence of 95% with theoretical results showing a high level of confidence. About 12,000 transitions were taken into account for the spectrum of Roncin et al. The relative intensities are presented as stated in reference [13], and the lines were convoluted with the measured apparatus profile. It is amazing to see the detailed similarity of the pattern of the energy levels between the experimental and the theoretical spectrum. Not only the vibrational but also numerous rotational transitions were identified in the spectrum of the cell. Similar to atomic emission, electronic transitions in low quantum numbers were preferred by the molecules in the plasma of the cell. However, the relative intensities of the spectrum in Figure 5(b) differed significantly from those of the spectrum of Roncin et al. in the range around 110 nm. This part of the spectrum belongs to a Werner band with $\upsilon' = 0$ and $\upsilon'' = 1$, respectively.

IV. Discussion

The emission of VUV radiation, and in particular, Lyman series and Werner band emission was observed from a low density plasma of quite moderate temperature similar to that in fluorescence tubes for general lighting. Such a plasma of an incandescently heated cell should not emit VUV radiation. The spectra showed that the plasma was far from thermal equilibrium. This was not too surprising because of the cell components, such as heater and titanium mesh etc., all may have contributed to a bimodal free-electron velocity distribution. But, the relevance of free electrons for the population of electronic levels is questionable

because of the preference for emission from a few specific electronic states of low quantum number. The same applies if a corona equilibrium was assumed.

Only blackbody radiation from the tungsten coil was observed at longer wavelengths. Based on the VUV emission, the plasma was predominately a hydrogen plasma. The ionization of atomic hydrogen requires 13.6 eV. In the cases where plasma was observed, no possible chemical reaction of the tungsten filament, the titanium screen, K_2CO_3, and low pressure hydrogen at a cell temperature of 750°C could be found which accounted for the generation and sustaining of the plasma. In fact, no known chemical reaction releases enough energy to form an atomic hydrogen plasma as treated in the following discussion.

The enthalpy of formation ΔH_p of potassium hydride is $-14.13\ kcal/mole$ [14]. Thus, the formation of potassium hydride releases only 0.59 eV per atom. But, potassium hydride decomposes in this temperature range (288 to 415°C). Thus, it can not account for any emission of the hydrogen plasma.

The reduction of K_2CO_3 by hydrogen calculated from the heats of formation is very endothermic.

$$H_2 + K_2CO_3 \rightarrow 2K + H_2O + CO_2 \quad \Delta H = +122.08\ kcal/mole\ H_2 \tag{1}$$

The reaction absorbs 2.5 eV per hydrogen atom.

The most energetic reaction possible with oxygen is the reaction of hydrogen to form water which releases 1.48 eV per atom of hydrogen; whereas, the energy of Lyman emission is greater than 10.2 eV per atom.

The dissociation of molecular hydrogen on the filament produces atomic hydrogen which may recombine to release 4.45 eV. Since atomic hydrogen is neutral, no contribution from the electric field of the filament is possible. Thus, excitation with energies of 4.45 eV or less is possible by the transport of thermal energy from the filament due to hydrogen dissociation followed by recombination. But this reaction is not sufficiently energetic to support the observed VUV emission.

Chemical energy may have been transported from regions outside of the annular region where most of the emission was observed. Dense and cold plasmas may have been created close to surfaces such as the titanium mesh due to chemical reactions. In such non ideal plasmas with electron densities close to solid density and temperatures below 0.5 eV, the potential energy of the electrons becomes comparable to their kinetic energy, and energy levels of bound electrons in atoms such as hydrogen are altered such that excitation and ionization energies are lowered [15]. This also applies to other elements of the plasma such as potassium. The electronic energy levels of the different species are further distorted when interacting with

each other. The dissociation of molecules and ionization of both the molecules and atoms may become more probable with more species. However, the lowering of the ionization and excitation energies by the state of "non ideality" in dense plasmas is only about 1 eV even for potassium. Thus, the most energetic chemical source possible, dissociated atomic hydrogen, could not have provided more energy than the Frank-Condon energy of 4.45 eV during recombination. Thus, this mechanism can not explain the hydrogen plasma.

The measured electron temperature, 0.5 eV, is over an order of magnitude too low to account for the hydrogen plasma. The filament electric field as the energy source of the excitation is also eliminated. The emission occurred even when the electric field was set and measured to be zero. The results can not be explained by electric field acceleration of charged species since the estimated external field of the incandescent heater is extremely weak, about 1 V/cm. The electron mean free path at the operating pressure range of 0.1 to 1 mbar is about 0.1 cm corresponding to a mean energy from the acceleration of electrons in the field of about 1 V/cm of under 1 eV. Thus, electron collisional excitation of Lyman emission or hydrogen ionization by a so called 'run-away-situation' of the velocities of free electrons is not probable. However, the observed plasma striations outside the titanium mesh close to the mesh points may have been due to local radial electric fields in the plasma not yet identified, where charged particles were accelerated in the dark zones to energies high enough to excite bound electrons in the brighter zones [11].

Temperature dependent electric fields also arise due to the greater mobility of electrons compared to ions. The generated voltage U for a plasma with a similar ion and electron temperature T is given by

$$U = \frac{kT}{2e} \ln \frac{m_x}{m_e} \tag{2}$$

where m_x is the mass of the ion such as the potassium ion or a proton, m_e is the electron mass, and e is the electron charge. From Eq. (2), the maximum voltage corresponding to the potassium ion is of the order of 1 V.

Multi-collisional processes may be possible [16], but very dense, high-pressure plasmas are required, and given an electron energy of 0.5 eV, about 30 concerted electron collisions would be required within 10^{-8} s—a definite impossibility.

Resonant energy transfer is possible to give predominantly Lyman α and Lyman β emission. Kurunczi, Shah, and Becker [17,18] observed intense emission of Lyman α and Lyman β radiation at 121.6 nm and 102.5 nm, respectively, from microhollow cathode discharges in high-pressure Ne (740 Torr) with the addition of a small amount of hydrogen (up

to 3 Torr). With essentially no molecular emission observed, Kurunczi et al. attributed the anomalous Lyman α emission to the near-resonant energy transfer between the Ne_2^* excimer and H_2 which leads to formation of $H(n = 2)$ atoms, and attributed the Lyman β emission to the near-resonant energy transfer between excited Ne^* atoms (or vibrationally excited neon excimer molecules) and H_2 which leads to formation of $H(n = 3)$ atoms. However, the formation of this plasma resulting in Ne_2^* excimers and excited Ne^* atoms required a field of over $10^4 V/cm$; whereas, the field in the heated cells is on the order of 1 V/cm. Thus, this mechanism does not provide a source of energetic photons that may be resonantly transferred.

The titanium-mesh and the tungsten coil were present in all experiments. The emission was not observed with the cell alone, with hydrogen alone, or under identical conditions wherein Na_2CO_3 replaced K_2CO_3. When the power was interrupted, the emission decayed in about two seconds. Decay was recorded over a time greater than 10,000 times the typical duration of a discharge plasma afterglow [19]. This experiment showed, that plasma emission was occurring even though the voltage between the heater wires was set to and measured to be zero for a time duration which was surprisingly extended. Since the thermal decay time of the filament for dissociation of molecular hydrogen to atomic hydrogen was similar to the plasma afterglow duration of the investigated source which requires the presence of K_2CO_3 the emission was determined to be due to a reaction of K_2CO_3 with atomic hydrogen. The minimum temperature requirement of the tungsten wire for emission also demonstrated the emission reaction's dependence on atomic hydrogen.

A source of energy other than that provided by the electric field or known chemical reactions must be considered for explaining our experimental findings.

V. Conclusion

The generation of the Lyman and Balmer series and the Lyman Werner bands of molecular hydrogen requires energies significantly greater than 10 eV. The formation of a hydrogen plasma by the cell loaded with K_2CO_3 on titanium and operated in hydrogen required a minimum temperature. The heat from the filament and possibly the weak dipole field from the filament may sustain the hydrogen plasma; but, the latter is not essential because hydrogen lines were emitted during times when this voltage is set to zero. Furthermore, given the observations, free electrons can not excite these states. In the case that the free electrons should have been thermalized, their temperature was too low to contribute to excitation or ionization even from the tail of the velocity distribution. Longer range fields (of the order of mm) were

only about a 1 V/cm. In addition to electron collisional excitation, known chemical reactions, and resonant photon transfer, the lowering of the ionization and excitation energies by the state of "non ideality" in dense plasmas were also rejected as the source of ionization or excitation to form the hydrogen plasma.

The emission from a plasma was observed at low temperatures (e.g. $\approx 10^3\ K$) from atomic hydrogen and potassium. The release of energy from hydrogen was evidenced by the hydrogen Lyman and Balmer emission which identified the presence of a hydrogen plasma. The persistence of emission following the removal of all of the power to the cell indicates that an unknown chemical power source is present. The implication is that a new plasma and light source for the vacuum ultraviolet has been discovered.

References

1. U. Kogelschatz, H. Esrom, J. Y. Zhang, I. W. Boyd, "High Intensity Sources of Incoherent UV and UVU Excimer Radiation for Low-Temperature Materials Processing", to be published in Appl. Surf. Sciences 2000/01.
2. A. Ohl, K. Schröder, "Plasma Induced Chemical Micropatterning for Cell Culturing Applications", Surface and Coating Technology, Vol. 116-119, (1999), p. 830.
3. B. Edlen, "Production of Highly Ionized Iron by a Vacuum Spark", Physica, Vol. 13, (1947), p. 545.
4. H. Conrads, "Die Erzeugung eines Rekombinationskontinuums mit Hilfe eines Gleitfunkens zur Bestimmung der absoluten Intensität im Vakuum-UV", Z. f. Physik, 200, (1967), p. 444.
5. K. H. Schoenbach, R. Verkeppen, T. Tassow, W. W. Byszewski, "Microhollow Cathode Discharges", Appl. Phys. Lett., Vol. 68, (1996), p. 13.
6. B. Eliasson, U. Kogelschatz, "UV Excimer Radiation from Electrical Barrier Discharges", Appl. Phys. B, Vol. 46, (1988), p. 299.
7. R. Mills, T. Onuma, and Y. Lu, "Formation of a Hydrogen Plasma from an Incandescently Heated Hydrogen-Catalyst Gas Mixture with an Anomalous Afterglow Duration", Int. J. Hydrogen Energy, Vol. 26, No. 7, July, (2001), pp. 749-7628.
8. R. Mills, J. Dong, Y. Lu, "Observation of Extreme Ultraviolet Hydrogen Emission from Incandescently Heated Hydrogen Gas with Certain Catalysts", Int. J. Hydrogen Energy, Vol. 25, (2000), pp. 919-943.

9. N. Ernst, J. H. Block, H. J. Kreuzer, X. Ye, "Thermal Field Desorption Spectroscopy of Chemisorbed Hydrogen for a Single Step Site", Phys. Rev. Lett., Vol. 71, (1993), p. 891.
10. F. Sigeneger, Yu. B. Golubovskii, I. A. Porokhova, R. Winkler, "On the Nonlocal Kinetics in s- and p-Striations of DC Glow Discharge Plasma: I. Electron Establishment in Striation-like Fields", Plasma Chemistry and Plasma Processing, Vol. 18, No. 2, (1998), p. 153.
11. F. Sigeneger, and R. Winkler, "On the Nonlocal Electron Kinetics in s and p Striations of a DC Glow Discharge Plasma: II. Electron Properties in Periodic States", Plasma Chemistry and Plasma Processing, Vol. 20, No. 4, (2000), p. 429.
12. W. L. Wiese, M. W. Smith, B. M. Glennon, "Atomic Transition Probabilities", Natl. Bur. Stand. (U.S.) No. NSRDS-NBS 4, U.S.~GPO, Washington, DC, Vol. I, (1966).
13. J. Y. Roncin, F. Launay, "Vacuum Ultraviolet Emission Spectrum of Molecular Hydrogen", J. Phys. Chem. Ref. Data, Monograph 4.
14. W. M. Muller, J. P. Blackledge, G. G. Libowitz, *Metal Hydrides*, Academic Press, New York, (1968), p. 201.
15. H. W. Darwin and P. Felenbok, "Data for Plasmas in Local Thermodynamic Equilibrium", Gauthier-Villars Ed., Paris, (1965).
16. P. Kurunczi, H. Shah, and K. Becker, "Excimer formation in high-pressure microhollow cathode discharge plasmas in helium initiated by low-energy electron collisions", International Journal of Mass Spectroscopy, Vol. 205, (2001), pp. 277-283.
17. P. F. Kurunczi, K. H. Becker, "Microhollow Cathode Discharge Plasma: Novel Source of Monochromatic Vacuum Ultraviolet Radiation", Proc. Hakone VII, Int. Symp. High Pressure, Low Temperature Plasma Chemistry, Greifswald, Germany, Sept. 10 - 13, (2000), Vol. 2, p. 491.
18. P. Kurunczi, H. Shah, and K. Becker, "Hydrogen Lyman-α and Lyman-β emissions from high-pressure microhollow cathode discharges in $Ne-H_2$ mixtures", J. Phys. B: At. Mol. Opt. Phys., Vol. 32, (1999), L651-L658.
19. A. Surmeian, C. Diplasu, C. B. Collins, G. Musa, I. Lovittz Popescu, J. Phys. D: Appl. Phys. Vol. 30, (1997), pp. 1755-1758.